The pressure-induced phase transition in SnO: a first-principles study

2007 J. Phys.: Condens. Matter 19 425230

(http://iopscience.iop.org/0953-8984/19/42/425230)

IOP PUBLISHING JOURNAL OF PHYSICS: CONDENSED MATTER

J. Phys.: Condens. Matter **19** (2007) 425230 (10pp) doi:10.1088/0953-8984/19/42/425230

The pressure-induced phase transition in SnO: a first-principles study

Y W Li, Y Li, T Cui, L J Zhang, Y M Ma[1] and G T Zou

National Laboratory of Superhard Materials, Jilin University, Changchun 130012, People's Republic of China

E-mail: mym@jlu.edu.cn

Received 3 August 2007
Published 18 September 2007
Online at stacks.iop.org/JPhysCM/19/425230

Abstract

The structural modifications of SnO within the tetragonal phase (α-SnO) and the orthorhombic phase (γ-SnO) with pressure were extensively studied by using the first-principles pseudopotential plane-wave method within the generalized gradient approximation. A structural phase transition from α-SnO to γ-SnO is predicted at 1.1 GPa by evaluating the enthalpy difference of the two crystal structures. During the transition, the volume changes continuously with increasing pressure, and a linear increase of the spontaneous strain is predicted. These facts indicated the second-order nature of this phase transition. Moreover, the pressure dependences of the Raman shift for both α-SnO and γ-SnO structures are presented to show further evidence for the phase transition. A softening B_{1g} mode with pressure is suggested to be the physically driven force of the transition. The current theoretical results strongly suggest the existence of γ-SnO phase in SnO under high pressure.

(Some figures in this article are in colour only in the electronic version)

1. Introduction

The tin oxides SnO and SnO_2 are of considerable technological interest [1]; in particular, SnO_2 is widely used in thin-film processes and technologies, (e.g. catalysis, gas sensing, heat reflection filters, transparent conducting coatings, and anode materials) [1, 2]. The physical and chemical properties of SnO_2 have been well studied, while SnO has received less attention due to its tendency to decompose at elevated temperature [2, 3].

Under ambient conditions SnO crystallizes in the tetragonal litharge structure α-SnO ($P4/nmm$, $Z = 2$), in which oxygen atoms occupy the Wyckoff 2a site while Sn atoms sit at the 2c site [2]. It is generally assumed that SnO is a semiconductor at ambient pressure [4] and it transforms to a metal at 5 GPa [1, 2]. An energy gap of about 2.5 eV has been quoted [5],

[1] Author to whom any correspondence should be addressed.

whereas the fundamental gap energy is given as 0.7 eV [4]. *Ab initio* calculations [6] showed that the energy gap is indirect (Γ to M in the Brillouin zone), and this was confirmed by later theoretical calculations [7, 8]. A pressure-induced phase transition in α-SnO has been experimentally reported [9–11]. The transition to a lower-symmetry orthorhombic γ-SnO ($Pm_{21}n$, $Z = 2$) phase was observed in the pressure range 1.5–2.5 GPa. But the recent experiments by Wang *et al* [2] and Giefers *et al* [12] did not show such a transition in this pressure range. It was suggested that the phase transition to the γ-SnO structure might be induced by nonhydrostatic conditions. However, the lack of theoretical studies impedes the understanding of this controversy. Thus, a theoretical study is motivated.

The current paper presents a detailed theoretical study on the pressure effect of SnO within two phases, α-SnO and γ-SnO, by means of *ab initio* calculations based on density-functional theory. Indeed, from the enthalpy difference calculation, we found that the orthorhombic structure of γ-SnO is energetically preferred beyond 1.1 GPa relative to the ambient tetragonal structure of α-SnO, strongly supporting the existence of the orthorhombic phase γ-SnO under pressure. A further lattice dynamic study suggested that B_{1g} mode softening is the physically driven force for this α-SnO to γ-SnO phase transition.

2. Theoretical methods

The *ab initio* calculations were performed within the density-functional theory (DFT) using the pseudopotential plane-wave method [13]. The method has already been used to predict accurately high-pressure structural, elastic, and vibrational properties of a large number of materials. We use the generalized gradient approximation (GGA) for the exchange–correlation potential within the Perdew–Burke–Ernzerhof (PBE) parameterization [14]. The Troullier–Martins [15] norm-conserving scheme is used to generate the tight pseudopotentials for Sn and O atoms with electronic configurations of $5s^25p^2$ and $2s^22p^4$, respectively. A convergence test gave the choice for the kinetic energy cutoff, E_{cutoff}, of 90 Ryd for both α-SnO and γ-SnO, and an 8 8 6 and 5 5 4 k mesh for α-SnO and γ-SnO, respectively in the electronic integration of the first Brillion zone. The structural optimization and the zone-center phonon calculations were calculated using the Quantum-ESPRESSO package [16]. The CASTEP code [17] was used to perform the calculation of the elastic constants of α-SnO.

The Raman intensities were computed from the second-order derivative of the electronic density matrix with respect to a uniform electric field [18]. In a Raman spectrum the peak intensity I^{υ} corresponding to an optical phonon ω_{υ} can be computed as

$$I^{\upsilon} \propto |e_i \cdot \overleftrightarrow{A}^{\upsilon} \cdot e_s|^2 \frac{1}{\omega_{\upsilon}}(n_{\upsilon} + 1), \tag{1}$$

where e_i (e_s) is the polarization of the incident (scattered) radiation,

$$\begin{aligned} n_{\upsilon} &= \left[\exp\left(\frac{\hbar\omega}{k_{\mathrm{B}}T}\right) - 1\right]^{-1}, \qquad \text{and} \\ A^{\upsilon}_{lm} &= \sum_{k\gamma} \frac{\partial^3 \varepsilon^{\mathrm{el}}}{\partial E_l \partial E_m \partial u_{k\gamma}} \frac{w^{\upsilon}_{k\gamma}}{\sqrt{M_{\gamma}}}. \end{aligned} \tag{2}$$

Here $\varepsilon^{\mathrm{el}}$ is the electronic energy of the system, E_l is the lth Cartesian component of a uniform electric field, $u_{k\gamma}$ is the displacement of the γth atom in the kth direction, M_{γ} is the atomic mass, and $w^{\upsilon}_{k\gamma}$ is the orthonormal vibrational eigenmode υ. According to the well-known Hellmann–Feynman theorem,

$$\frac{\partial^3 \varepsilon^{\mathrm{el}}}{\partial E_l \partial E_m \partial u_{k\gamma}} = 2\,\mathrm{Tr}\left\{\left(\frac{\partial^2 \rho}{\partial E_l \partial E_m}\right)\frac{\partial V^{\mathrm{ext}}}{\partial u_{k\gamma}}\right\}, \tag{3}$$

Table 1. Calculated equilibrium structural parameters (a_0, c/a, z_0), volume (V_0), bulk modulus (B_0), and the pressure derivative of bulk modulus (B_0') for α-SnO, and compared with experimental results from [2, 9, 19] and [21] and other theoretical results from [6] and [20]. z_0 is the atomic position of the Sn atom and V_0 is the volume per unit cell.

	a_0 (Å)	c/a	z_0	V_0 (Å^3)	B_0 (GPa)
This study	3.8469	1.2782	0.2341	72.72	31
Expt.[a]	3.7986	1.2744	0.2389	69.85	38
Expt.[b]	3.8029	1.2722	0.2383	69.97	50[c], 51[d]
Reference [6]	3.797	1.225	0.2404	67.06	35
Reference [20]	3.867	1.3023	0.234	74.50	

[a] Reference [2].
[b] Reference [19].
[c] Reference [9].
[d] Reference [21].

Table 2. Comparison of the calculated and measured lattice constants a, b, c and V (volume per formula unit) of γ-SnO at 2.57 GPa; the measured values were taken from [9].

	a (Å)	b (Å)	c (Å)	V (Å^3)
This work	3.821	3.810	4.619	33.63
Expt.[a]	3.805	3.785	4.613	33.22

[a] Reference [9].

where the DFT density matrix $\rho = \sum_\nu |\psi_\nu\rangle\langle\psi_\nu|$, $\langle\psi_\nu|$ being the normalized occupied Kohn–Sham (KS) eigenstates, Tr$\{O\}$ is the trace of the operator O, and V^{ext} is the external ionic potential.

3. Results and discussions

The cell parameters and atomic positions of the tetragonal and orthorhombic structures of SnO were fully optimized at selected pressures. The comparison of the theoretical and experimental [2, 19] structural parameters for α-SnO at zero pressure and γ-SnO at 2.57 GPa is given in tables 1 and 2, respectively. It is found from table 1 that all structural parameters were in excellent agreement with the experimental measurements within 1.2% except for the equilibrium volume, which is calculated to be 4% larger than the observed value. For γ-SnO, the calculated lattice constants a, b, c and V (volume per formula unit) are also in excellent agreement with the experimental data [9] as listed in table 2, the deviation between the theory and experiment being less than 0.7%. The overestimation of the theoretical lattice constants for both phases is a typical deviation of the GGA.

The computational approach employed here is based on constant-pressure static quantum-mechanical calculations at the thermal limit ($T = 0$ K), where the free energy is replaced by the enthalpy ($H = E + pV$) [22]. The calculated enthalpy of both tetragonal α-SnO and orthorhombic γ-SnO is presented in figure 1. One can observe that beyond 1.1 GPa the orthorhombic γ-SnO is more energetically favorable, indicating that there exists a phase transition from α-SnO to γ-SnO at $\sim$1.1 GPa. However, it is worth mentioning that, in the pressure range between 0.7 and 1.1 GPa, the energy differences are too small to distinguish. It is also found that at a pressure below 1.1 GPa, the orthorhombic phase always relaxes spontaneously back to the tetragonal structure. It is very important to note that the changes of the cell volumes with pressure from α-SnO to γ-SnO at 1.1 GPa are continuous, as shown

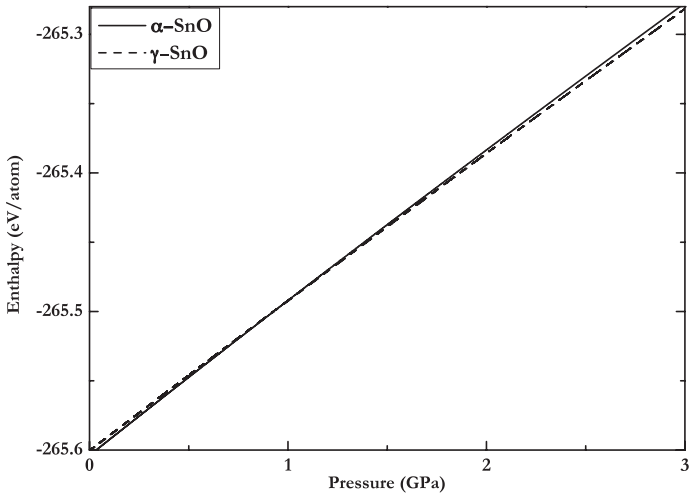

Figure 1. The calculated free energy (enthalpy $H = E + PV$) as a function of pressure for tetragonal α-SnO (solid line) and the orthorhombic γ-SnO (dashed line).

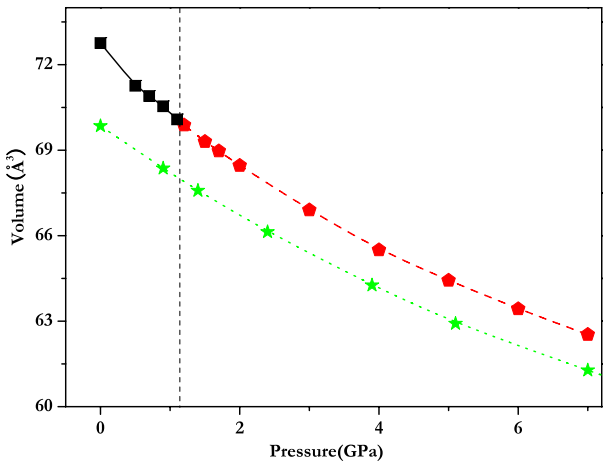

Figure 2. Calculated pressure–volume data for α-SnO (solid (black) square) and γ-SnO (solid (red) diamond) together with experimental data (solid (green) stars) taken from [2] for α-SnO. The vertical dashed line at 1.1 GPa is a border for the α-SnO to γ-SnO phase transition. The lines through the data points are the B-Spline fits.

in figure 2, suggesting a second-order nature for this phase transition. This fact is in excellent agreement with the experimental suggestion [9].

All zone-center phonon modes (three acoustic and nine optic) for α-SnO and γ-SnO were calculated in the pressure range of 0 to 8 GPa. Three modes with zero frequencies were assigned to the acoustic modes as expected. The calculated eigenvectors were used to deduce the symmetry labels of the particular modes. The α-SnO optic modes have the following irreducible representations:

$$\Gamma_{\text{Tetra}} = {A_{1g}}^{R} + {A_{2u}}^{IR} + {B_{1g}}^{R} + 2{E_g}^{R} + {E_u}^{IR} \tag{4}$$

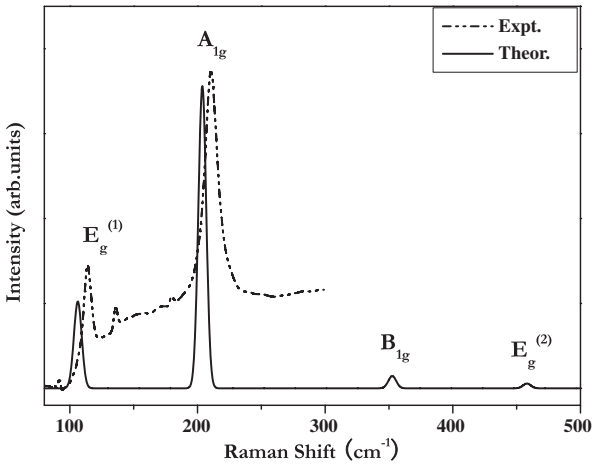

Figure 3. The comparison of calculated (solid line) Raman spectra of α-SnO at 0 GPa with the available experiment results (dashed–dotted line) taken from [2]. The calculated spectra are convoluted with a uniform Gaussian broadening with a 2.5 cm^{-1} width.

Table 3. The calculated frequencies and linear pressure coefficients ($d\omega/dP$) of the Raman modes for α-SnO and γ-SnO along with the experimental results from [2] and [5], and another theoretical result from [23] for α-SnO. The correlations of Raman modes between two phases are also listed.

α-SnO (0 GPa)			γ-SnO (1.5 GPa)		
Modes	ω (cm^{-1})	($d\omega/dP$) (cm^{-1} GPa^{-1})	Modes	ω (cm^{-1})	($d\omega/dP$) (cm^{-1} GPa^{-1})
$E_g^{(1)}$	107 (113[a])	2.0 (2.1[b])	B_1	111	2.2
			A_2	111	2.4
A_{1g}	204 (212[a], 211[c])	2.25 (2.4[b])	A_1	207	2.2
B_{1g}	350 (350[a], 113[c])	−11.11	A_1	340	3.4
$E_g^{(2)}$	446 (460[a])	15.56	A_2	467	6.8
			B_1	467	7.0

[a] Reference [23]
[b] Reference [2].
[c] Reference [5].

whereas the γ-SnO optic modes take the irreducible representations

$$\Gamma_{\text{Ortho}} = {A_1}^R + 2{A_2}^R + 3{B_1}^R + B_2^R. \tag{5}$$

The symbols A and B represent non-degenerate vibrational modes, and E doubly degenerate modes. Raman-active modes are labeled by the superscript R and infrared-active ones by IR. The calculated Raman spectra of α-SnO at 0 GPa along with the available experiment results [2] are shown in figure 3. In experiment, only low-frequency $E_g^{(1)}$ and A_{1g} modes have been observed, while the other two modes, B_{1g} and $E_g^{(2)}$, are not identified. From figure 3, it is clear that the calculated spectral intensity and peak positions of $E_g^{(1)}$ and A_{1g} modes are in excellent agreement with the experimental measurements [2] with only small red shifts of 6 and 8 cm^{-1}, respectively. In addition, it is predicted that the intensities of the B_{1g} and $E_g^{(2)}$ modes are very weak relative to those of $E_g^{(1)}$ and A_{1g} modes. In real experiments, a Raman peak with very weak intensity may not be properly detected. Therefore, this fact is mainly responsible for the failure of the observation of the B_{1g} and $E_g^{(2)}$ modes in experiments. Table 3 lists the calculated frequencies and the linear pressure coefficients of the Raman modes for the two phases along

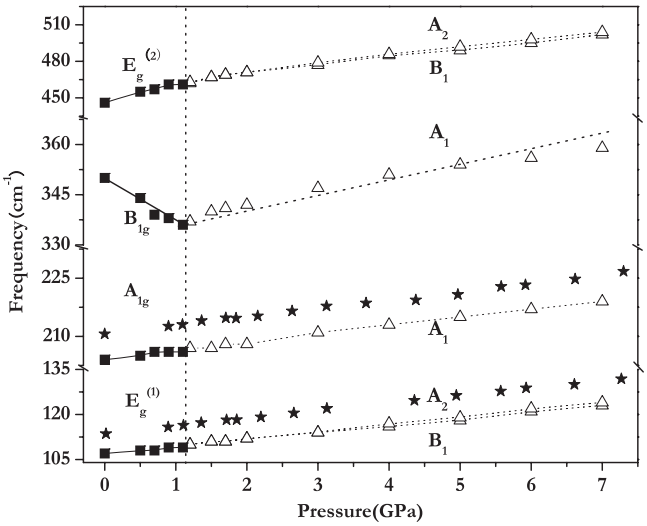

Figure 4. The theoretical pressure dependence of the Raman frequencies of α-SnO (solid squares) and γ-SnO (open triangles) along with the experimental data (solid stars) from [2] of the $E_g^{(1)}$ and A_{1g} modes for α-SnO. The dotted vertical line at 1.14 GPa denotes the transition from tetragonal α-SnO to orthorhombic γ-SnO.

with the experimental [2, 5] and previous theoretical [23] results at zero pressure for α-SnO. One observes that the calculated Raman frequencies at zero pressure are in excellent agreement with previous theoretical results [23]. It is noteworthy that the two theoretical frequencies for the A_{1g} mode agree well with the experimental measurement. However, the two calculated frequencies for B_{1g} mode are three times larger than the experimental value of 113 cm^{-1}. It should be pointed out that the assignment of the frequency 113 cm^{-1} to the B_{1g} mode had been proved to be incorrect by Peltzer *et al* [6], in which it was suggested to be the $E_g^{(1)}$ mode. The currently calculated frequency of the $E_g^{(1)}$ mode is 107 cm^{-1}, which coincides with the experimental value of 113 cm^{-1}. The current calculation strongly supports the conclusion of Peltzer *et al*'s [6].

Figure 4 shows the calculated pressure dependence of the Raman mode frequencies of α-SnO (solid squares) and γ-SnO (open triangles) along with the experimental data (solid stars) for α-SnO. In the α-SnO phase, it is found that A_{1g}, $E_g^{(1)}$, and $E_g^{(2)}$ increase with pressure, while the B_{1g} mode has a softening behavior below 1.14 GPa. All Raman frequencies of γ-SnO increase with pressure above 1.14 GPa. The theoretical linear pressure coefficients for the four modes in α-SnO are also listed in table 3. It is clear that the theoretical coefficients for the $E_g^{(1)}$ and A_{1g} modes are in excellent agreement with the experimental data [2]. The mode Grüneisen parameters for $E_g^{(1)}$ and A_{1g} modes have also been calculated. The calculated values of $\gamma(E_g^{(1)}) = 0.65$ and $\gamma(A_{1g}) = 0.30$ are also in satisfactory agreement with the experimental measured results [2] of $\gamma(E_g^{(1)}) = 0.80(8)$ and $\gamma(A_{1g}) = 0.38(4)$. It is important to note that the theoretical linear pressure coefficient for the B_{1g} mode in α-SnO is calculated to be -11.11 cm^{-1} GPa^{-1}, indicating a pressure-induced soft mode. There is a crossing point between the softening B_{1g} mode in α-SnO and the hardening A_1 mode in γ-SnO at 1.14 GPa. Beyond 1.14 GPa, a hardening behavior of the A_1 mode in γ-SnO is evidenced. This behavior implies the existence of the α–γ phase transition of SnO. The predicted transition pressure corresponding to the crossing point is $\sim$1.14 GPa, which by accident coincides with the transition pressure of 1.1 GPa in the enthalpy calculation.

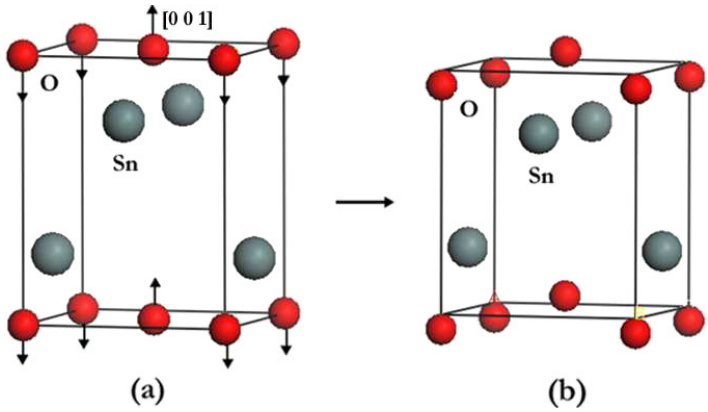

Figure 5. A schematic representation of the transition path from the tetragonal to the orthorhombic phase. (a) The eigenvectors of the tetragonal B_{1g} mode. All Sn cations remain fixed while the O anions vibrate along the [001] and [00$\bar{1}$] directions. (b) The orthorhombic phase is formed with the instability of O atomic motions.

The schematic representation of eigenvectors for the soft B_{1g} Raman mode of the tetragonal phase is shown in figure 5(a). The arrows represent the directions of the atomic vibrations. It is found that all the Sn cations remain fixed, while the O anions vibrate along the [001] and [00$\bar{1}$] directions. The instability of such atomic motions could easily break the tetragonal symmetry of the system, and thus, tend to form the new orthorhombic phase as shown in the figure 5(b). This behavior is similar to that of the soft-mode induced phase transitions in many metal dioxides, such as SiO_2 [24, 25], SnO_2 [26] and CrO_2 [27]. It is noteworthy that at the transition pressure of 1.14 GPa, with the exception of the B_{1g} mode, the variations of the other three modes with pressure are continuous, as shown in figure 4. Therefore, one would not discover this phase transition by simply probing only A_{1g} and $E_g{}^{(1)}$ Raman modes in the experiments. This fact might contribute to the failure of the observation of the phase transition in the Raman measurements by Wang *et al* [2].

As in the case of SiO_2, there is also a pressure-induced instability in the elastic constant with the Raman mode softening. Thus, we also performed an elastic constants calculation in the α-SnO phase. However, as plotted in figure 6, the values of C_{11}, C_{12}, C_{44}, C_{66} and shear modulus $C_{sm} = (C_{11} - C_{12})/2$ all show a linear increase with pressure up to 1.2 GPa. This fact suggests that there is no elastic instability developing with the soft-mode phase transition of SnO.

The structure of α-SnO is layered with an $AA\ldots$ stacking sequence of slabs, and each Sn atom is at the apex of a square pyramid whose base is formed by four oxygen atoms [28]. The single O–O (2.69 Å) and four Sn–O bond lengths (2.22 Å) in a square pyramid together with the distances between Sn atoms in both intralayers and interlayers have been experimentally studied [2]. The calculated interatomic distances for α-SnO and γ-SnO as a function of pressure are presented in figure 7. One observes that the calculated results for α-SnO agree well with the experimental data. At the theoretical transition pressure of 1.14 GPa, the interatomic distances change continuously from α-SnO to the γ-SnO phase except for the O–O bond, which has a small increase from 2.709 Å in α-SnO to 2.712 Å in γ-SnO. This increase of the O–O bond might be induced by the soft B_{1g} mode in α-SnO, which consists of buclking vibrations of the O atoms out of their plane along the c axis [6]. In addition, the Sn–O bond splits into two different bonds at the transition, indicating that the square pyramid formed by one Sn atom and four O atoms in α-SnO distorts with pressure.

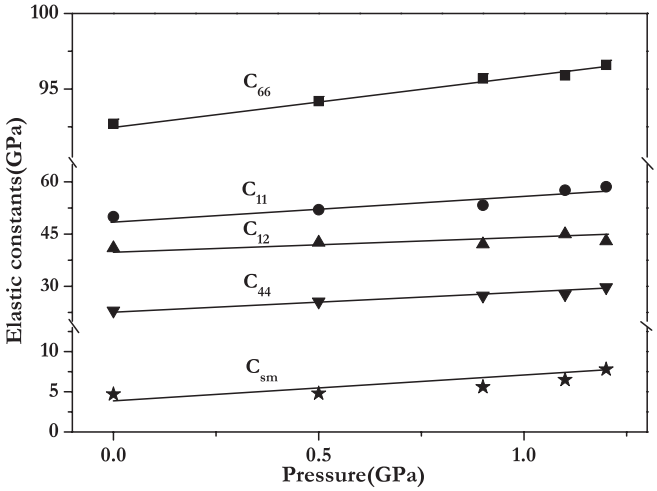

Figure 6. The calculated elastic constants C_{11}, C_{12}, C_{44}, C_{66} and C_{sm} plotted against pressure for α-SnO. The solid lines are the linear fits to the calculated results.

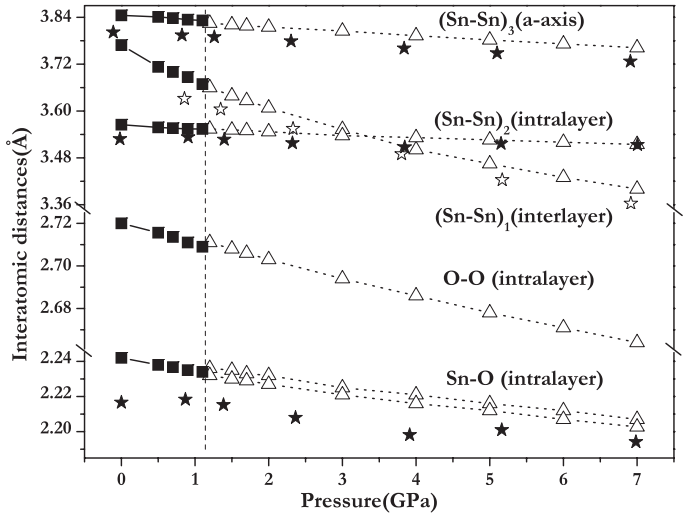

Figure 7. Calculated interatomic distances of α-SnO (solid squares) and γ-SnO (open triangles); solid and open stars represent experimental results from [2]. The dotted vertical line at ∼1.14 GPa denotes the transition from tetragonal α-SnO to orthorhombic γ-SnO.

It is often difficult to correctly determine the order of a phase transition [27]. Indeed, in many other oxides [9, 27], the transitions from the tetragonal to orthorhombic structure have been shown to be second order with the spontaneous strain, $e_{ss} = (a-b)/(a+b)$, as the order parameter. According to the Landau theory of second-order phase transitions [27, 29], the order parameter should be proportional to $(P - P_c)^{1/2}$. To examine this possibility, we have plotted e_{ss}^2 versus pressure in figure 8. The data show an almost perfect linear increase up to 3 GPa, suggesting that the transition from α-SnO to γ-SnO is of a second-order nature. This behavior agrees well with our equation of states calculation. The extrapolation of the linearly fitted

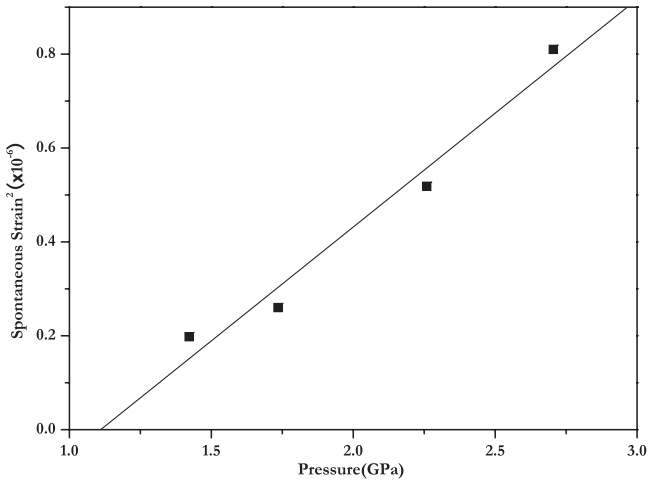

Figure 8. The calculated spontaneous strain (solid squares) for γ-SnO defined as $(a-b)/(a+b)$; the solid line through the calculated data is a linear fit.

curve to zero of e_{ss}^2 gives a value of the transition pressure as 1.08 GPa, which is in excellent agreement with those of 1.14 and 1.15 GPa in the soft-mode and enthalpy calculations.

4. Conclusion

In conclusion, the pressure-induced phase transition from tetragonal α-SnO to orthorhombic γ-SnO was studied using density-functional linear-response theory. The phase transition occurs at 1.1 GPa, as suggested by the free-energy calculations, and was testified to be of second order in character from the continuous change in volume at the transition and the linear increase of the spontaneous strain. The calculated transition pressure of 1.1 GPa is in excellent agreement with the experimental values of 1.5–2.5 GPa [9–11]. The Raman analysis indicates a softening behavior of the B_{1g} mode, which is suggested to be responsible for the α–γ phase transition in SnO.

Acknowledgments

We are grateful for the financial support of the China 973 Program under Grant No. 2005CB724400, the NSAF of China under Grant No. 10676011, the National Doctoral Foundation of China Education Ministry under Grant No. 20050183062, the SRF for ROCS, SEM, the Program for 2005 New Century Excellent Talents in University, and the 2006 Project for Scientific and Technical Development of Jilin Province.

References

[1] Christensen N E, Svane A and Peltzer y Blancá E L 2005 *Phys. Rev.* B **72** 014109
[2] Wang X, Zhang F X, Loa I, Syassen K, Hanfland M and Mathis Y L 2004 *Phys. Status Solidi* b **241** 3168
[3] Moreno M S and Mercader R C 1994 *Phys. Rev.* B **50** 9875
[4] Krishna K M, Sharon M, Mishra M K and Marathe V R 1996 *Electrochim. Acta* **41** 1999
[5] Geurts J, Rau S, Richter W and Schmitte F J 1984 *Thin Solid Films* **121** 217

[6] Peltzer y Blanca E L, Svane A, Christensen N E, Rodriguez C O, Cappannini O M and Moreno M S 1993 *Phys. Rev.* B **48** 15712
[7] Lefebvre I, Szymanski M A, Olivier-Fourcade J and Jumas J C 1998 *Phys. Rev.* B **58** 1896
[8] Raulot J M, Baldinozzi G, Sashadri R and Cortona P 2002 *Solid State Sci.* **4** 467
[9] Adams D M, Christy A G, Haines J and Clark S M 1992 *Phys. Rev.* B **46** 11358
[10] Ssrebryaya N R, Kabalkina S S and Vereshchagin L F 1969 *Dokl. Akad. Nauk SSSR* **187** 307
[11] Suito K, Kawai N and Masuda Y 1975 *Mater. Res. Bull* **10** 677
[12] Giefers H, Porsch F and Wortmann G 2006 *Physica* B **373** 76
[13] Baroni S, Giannozzi P and Testa A 1987 *Phys. Rev. Lett.* **58** 1861
[14] Perdew J P and Burke K 1996 *Int. J. Quantum Chem.* **57** 309
[15] Troullier N and Martins J L 1991 *Phys. Rev.* B **43** 1993
[16] Baroni S *et al* http://www.pwscf.org
[17] Segall M D, Lindan P L D, Probert M J, Pickard C J, Hasnip P J, Clark S J and Payne M C 2002 *J. Phys.: Condens. Matter* **14** 2717
[18] Lazzeri M and Mauri F 2003 *Phys. Rev. Lett.* **90** 036401
[19] Pannetier J and Denes G 1980 *Acta Crystallogr.* B **36** 2763
[20] Walsh A and Watso G W 2004 *Phys. Rev.* B **70** 235114
[21] Vereshchagin L F, Kabalkina S S and Lityagina L M 1966 *Dokl. Akad. Nauk SSSR* **163** 326
[22] Catti M 2005 *Phys. Rev.* B **72** 064105
[23] Koval S, Burriel R, Stachiotti M G, Castro M, Migoni R L, Moreno M S, Varela A and Rodriguez C O 1999 *Phys. Rev.* B **60** 14496
[24] Karki B B, Warren M C, Stixrude L, Ackland G J and Crain J 1997 *Phys. Rev.* B **55** 3465
[25] Kingma M J, Cohen R E, Hemley R J and Mao H K 1995 *Nature* **374** 243
[26] Hellwig H, Goncharov A F, Gregoryanz E, Mao H K and Hemley R J 2003 *Phys. Rev.* B **67** 174110
[27] Maddox B R, Yoo C S, Kasinathan D, Pickett W E and Scalettar R T 2006 *Phys. Rev.* B **73** 144111
[28] Terra J and Guenzburger D 1991 *Phys. Rev.* B **44** 8584
[29] Haines J and Leger J M 1997 *Phys. Rev.* B **55** 11144